Nano Research

Open Access

Research Article

Dynamic liquid film nanochannels for adjustable ion and molecule transport

Chunxiao Liang[1,2], Dianyu Wang[3], Zhe Xu[1], Haitao Deng[1,2], Fan Xia[4], and Ye Tian[1,2,5,6] ✉

[1] *Key Laboratory of Bioinspired Materials and Interfacial Science, Technical Institute of Physics and Chemistry, Chinese Academy of Sciences, Beijing 100190, China*
[2] *University of Chinese Academy of Sciences, Beijing 100049, China*
[3] *School of Chemical Engineering, Zhengzhou University, Zhengzhou 450001, China*
[4] *State Key Laboratory of Biogeology and Environmental Geology, Engineering Research Center of Nano-Geomaterials of Ministry of Education, Faculty of Materials Science and Chemistry, China University of Geosciences, Wuhan 430074, China*
[5] *Suzhou Institute for Advanced Research, University of Science and Technology of China, Suzhou 215123, China*
[6] *Qingdao Institute of Bioenergy and Bioprocess Technology, Chinese Academy of Sciences, Qingdao 266101, China*

Cite this article: *Nano Research*, **2025**, *18*, 94907256. https://doi.org/10.26599/NR.2025.94907256

ABSTRACT: Gating, a fundamental feature of biological nanochannels, enables the intelligent regulation of ion and molecule transport in response to specific requirements. Inspired by nature, numerous artificial gating systems have been researched through the functionalization of solid-state nanochannels. However, these gating systems typically allow only two transitions: "open" and "closed", which makes it challenging to achieve multi-state transport. Herein, we construct dynamic liquid film nanochannels (DLFNs) by inserting an oil droplet into a capillary with gradient wettability that is filled with ionic solutions. The liquid film, formed between the oil and the capillary, functions as a nanochannel for ion and molecule transport, with its height dynamically adjusted through the capillary's gradient wettability. At a deeper level, the variations in liquid film thickness are driven by the interfacial water structure, which is mediated by hydrogen bonding interactions. Furthermore, unlike traditional solid-state nanochannels, which involve two phases (liquid/solid), the properties of DLFNs are influenced by three phases (oil/water/solid), resulting in distinct performance characteristics, such as reconfigurability, low cost, and ease of fabrication. This work provides an avenue for designing dynamic nanofluids and may spark promising applications of DLFNs with multiscale gating properties in drug delivery, microreactors, sieving, biosensing, and other related fields.

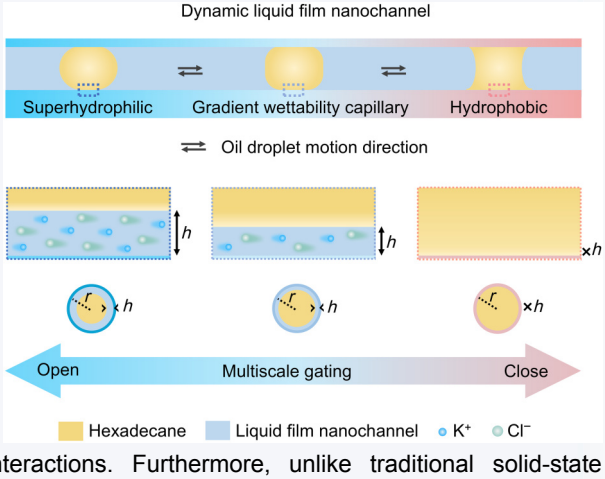

KEYWORDS: dynamic liquid film, nanochannel, gating, wettability, oil–water–solid interface

1 Introduction

Nanochannel multiscale gating systems show broad applications in micro- and nano-fluidics [1], controlled drug delivery [2], microreactors [3], separations [4], sensing [5–7], and other areas. For instance, controlling the pore size of nanochannels can regulate the transport rate of drug molecules, enabling precise drug delivery [2]. In addition, it can be used to modulate the transport rate of reactant molecules, thereby controlling the reaction rate and generating specific products [3]. Gating is also widely used for separating particles [8], ions [9], and molecules [10, 11] of different sizes, with widespread applications in water treatment, separation processes, and purification.

Currently, surface charge [12–14], wettability [15–18], and size [19–21] of nanochannels have been reported as the main factors for regulating gating. However, due to the limited efficiency of surface modification in solid-state nanochannels, gating transitions typically occur between two distinct states: "open" and "closed". Additionally, the fabrication of solid-sate nanochannels is complex and costly, which restricts their broad development. Consequently, achieving precise multiscale control over the dynamic gating

Received: December 11, 2024; **Revised:** January 7, 2025
Accepted: January 13, 2025

✉Address correspondence to tianyely@iccas.ac.cn

process in a simple and economical way remains challenging. Liquid film nanochannels, an alternative form of nanofluids, can be constructed within glass capillaries [22–24], which offer advantages such as adjustable nanochannel height, simple fabrication, and low cost. Furthermore, glass capillaries with millimeter-scale pore sizes offer large modification capacity, enabling efficient and complex modifications, such as gradient wettability, thereby conferring richer functionality to the nanochannels. Herein, we fabricate dynamic liquid film nanochannels (DLFNs) by injecting an oil droplet (hexadecane, unless otherwise specified) into a glass capillary filled with an ionic solution (Fig. 1). The liquid film formed between the oil and the capillary serves as a nanochannel, with its thickness dynamically adjusted by positioning the oil droplet within gradient wettability regions of the capillary (Fig. 1(a)). Specifically, when the oil droplet is positioned in the superhydrophilic region, a thicker liquid film forms between the oil and the capillary, resulting in an open state. As the oil droplet being moved to the hydrophobic region, the thickness of the liquid film decreases to zero, resulting in a closed state. Furthermore, DLFNs can be used to achieve multiscale gating for regulating ion transport over a broad range (Fig. 1(b)). Therefore, by constructing capillaries with gradient wettability and positioning the oil droplet at various wettability regions, DLFNs can be created, enabling multiscale gating for the controlled transport of ions and molecules. This system holds potential applications in controlled drug delivery, chemical reaction rate regulation, separation, purification, and other related fields.

2 Experimental sections

2.1 Materials

Potassium chloride (KCl), hydrogen peroxide (H_2O_2, 30 wt.%), hydrochloric acid (HCl, 37 wt.%) and ethanol were purchased from Sinopharm Chemical Reagent Co., Ltd. Sodium hydroxide (NaOH) was purchased from Sigma-Aldrich. Hexadecane was purchased from Macklin. Acetic acid, fluorescein sodium, n-octanoic acid, n-octanol and toluene were purchased from Aladdin. The modified silanes: 3-Mercaptopropyltriethoxysilane ($(CH_3CH_2O)_3SiC_3H_6SH$), 3-(triethoxysilyl)propylsuccinic anhydride, 3-aminopropyltriethoxysilane ($(CH_3CH_2O)_3SiC_3H_6NH_2$, abbreviated as -$NH_2$), 3-methacryloxypropyltrimethoxysilane ($(CH_3O)_3Si(CH_2)_3OCOC_3H_5$, abbreviated as -CO), and 1H,1H,2H,2H-perfluorooctyl trimethoxysilane ($CF_3(CF_2)_5CH_2CH_2Si(CH_3O)_3$, abbreviated as -CF) were purchased from Aladdin. All purchased reagents were used as received without any further purification. Glass capillaries were purchased from the Instrument Factory of West China Medical University with inner diameters of 0.9–1.1 mm.

2.2 Fabrication of the liquid film nanochannel

The ionic solution was first injected into a glass capillary using a syringe, followed by the injection of 1 μL of oil with a microsyringe, thereby constructing a liquid film nanochannel. It is important to note that no air bubbles were introduced during the injection process. To create dynamic liquid film nanochannels, we used a syringe to inject the electrolyte into the capillary, which pushed the oil droplet to the desired location. During the experiment, we ensured that the capillary remained horizontal to prevent displacement of the oil droplet by gravity. Additionally, the position of the oil droplet was marked prior to the test, and the droplet remained virtually stationary at the marked position after the experiment.

2.3 Modifications of functional molecules on glass surfaces

Surface wettability can be regulated by chemically grafting functional molecules. Firstly, glass plates were soaked in 0.1 M NaOH solution for 2 h, rinsed with deionized water. Then, they were soaked in 0.1 M HCl aqueous solution for 5 min and rinsed with deionized water to obtain superhydrophilic substrates (–OH). To obtain substrates with sulfonic acid groups (–SO_3H) [25], a 4% (v/v) solution of 3-mercaptopropyltriethoxysilane in ethanol was used to treat the superhydrophilic substrates (–OH) for 12 h to obtain sulfydryl surfaces (–SH). After that, these substrates (–SH) were washed with ethanol and blown dry with nitrogen. Later, these substrates were treated with H_2O_2/CH_3COOH (v/v = 1:1) for another 12 h to modify sulfonic acid groups (–SO_3H). To obtain

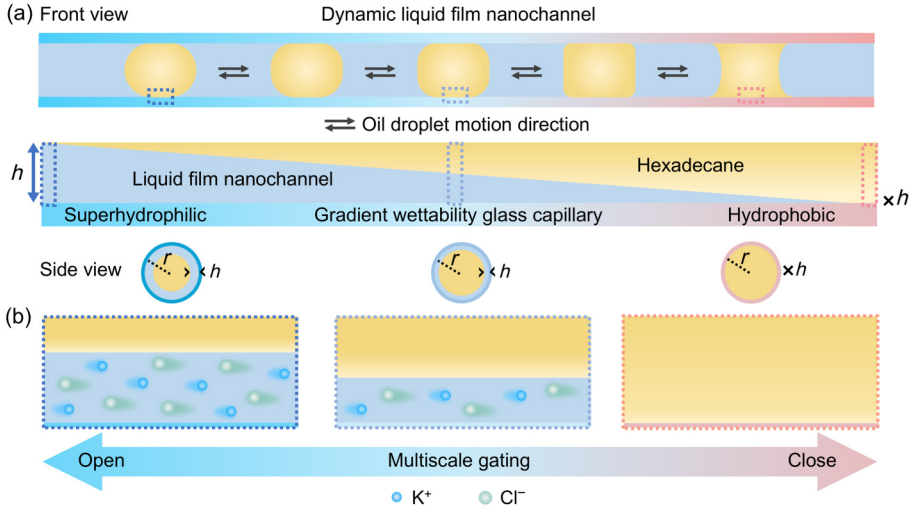

Figure 1 Design of DLFNs. (a) Schematic diagram of DLFNs constructed based on an oil–water–solid three-phase system. The height of the liquid film nanochannel can be dynamically regulated by the gradient wettability of the glass capillary. (b) Schematic diagram of multiscale gating in liquid film nanochannels. When the oil droplet is positioned in the superhydrophilic region, a thicker liquid film forms between the oil and the capillary, resulting in an open state. As the oil droplet moves to the hydrophobic region, the thickness of the liquid film decreases to zero, resulting in a closed state.

substrates with carboxyl groups (–COOH) [12, 26], superhydrophilic substrates were soaked in an ethanol solution containing 1 vol.% 3-(triethoxysilyl)propylsuccinic anhydride and 5 vol.% water for 12 h at room temperature, rinsed with ethanol and blown dry with nitrogen. To obtain substrates with amino groups ($-NH_2$), superhydrophilic substrates were immersed in an ethanol solution containing 2 vol.% 3-aminopropyltriethoxysilane for 12 h at room temperature, rinsed with ethanol and blown dry with nitrogen. Hydrophobic substrates (–CO and –CF) [27] were obtained by silanizing superhydrophilic substrates with 3-methacryloxypropyltrimethoxysilane and 1H,1H,2H,2H-perfluorooctyltrimethoxysilane evaporation in a decompression environment (~ 0.2 atm) at 120 °C for 4 h.

2.4 Ionic current recordings

The glass capillary was mounted between two polytetrafluoroethylene (PTFE) chambers filled with KCl solution. Ag/AgCl electrodes were used to apply a transmembrane potential across the liquid film nanochannels. Scanning current–voltage (*I*–*V*) experiments were carried out with transmembrane potentials varying from –1.0 to +1.0 V during a 21 s period using a Keithley 6487 Picoammeter (Keithley Instruments, Cleveland, OH, USA).

2.5 Measurement of zeta potentials

The zeta potentials of glass surfaces were measured using a SurPASS 3 electrokinetic analyzer (Anton Paar) with an adjustable gap cell. For each surface, two 1 cm × 2 cm glass pieces were attached in the cell with a 100 μm gap height parallel to each other. The zeta potentials at the oil–water interface were measured using a zeta potential analyzer (NanoZS, Malvern, UK). Mixtures containing 2 vol.% hexadecane in ion solution were sonicated in an ultrasonic homogenizer (JY92-IIN, Scientz, China) at 90% power for 1 min to form emulsions. Subsequently, these mixtures were diluted with ion solution to 0.1 vol.%.

2.6 Characterization

Contact angles were measured using a contact angle system (OCA20, DataPhysics Instruments, Germany) at room temperature. The droplet volume was approximately 2 μL. For each sample, five measurements were conducted at different positions. The adhesive force was measured using a high-sensitivity microelectromechanical balance system (DCAT11, DataPhysics Instruments, Germany). The surface roughness was measured using an atomic force microscope (Dimension FastscanBio, Bruker, USA). Microscope images were captured on an optical microscope (Vision Engineering Co.) coupled with a CCD camera (DP80, Olympus, Japan). Fluorescent spectra were obtained by using a fluorescence spectrometer (RF-5301PC, Shimadzu, Japan). Attenuated total reflection infrared (ATR-IR) spectra were obtained by a Fourier transform infrared (FTIR) spectrometer (INVENIO-S, Germany). The wavenumber range was from 4000 to 2800 cm^{-1}, the resolution was 4 cm^{-1} with 24 scans.

3 Results and discussion

To explore the influence of wettability on liquid film nanochannels, we modified the capillary walls with different groups to regulate their wettability (Fig. 2). It has been demonstrated that glass can achieve superhydrophilicity when treated with alkali [28]. This occurs because blank glass mainly contains oxygen bridges (Si–O–Si), while alkali-treated glass is rich in hydroxyl groups (Si–OH), resulting in superhydrophilicity [29–32]. Using this principle, we soaked flat glass plates in a 0.1 M NaOH solution for various durations and measured the water contact angles on the glass. The results show that as the treatment duration increases, the water contact angles on glass gradually decrease, stabilizing at around 6° after 60 min (Fig. 2(a)). To investigate the effect of wettability on liquid film nanochannels, we soaked capillaries in a 0.1 M NaOH solution for varying durations. The schematic of the experimental setup for recording ion conductance is presented in Fig. S1 in the Electronic Supplementary Material (ESM). The capillary is mounted between two PTFE containers filled with KCl solution, and Ag/AgCl electrodes are inserted into the KCl solution to apply a transmembrane voltage (unless specially described, the concentration of KCl solution is 0.1 M). The results indicate that longer soaking durations lead to a gradual increase in the ion conductance of the liquid film nanochannels, stabilizing at around 4×10^{-7} S after 60 min (Fig. 2(b) and Fig. S2 in the ESM). The stability of ion transport through the liquid film nanochannel constructed in superhydrophilic capillary was evaluated using a 0.1 M KCl solution. Alternating the external bias between +0.1 and –0.1 V showed that both the negative and positive currents exhibited minimal fluctuation in each cycle, indicating stable ion transport behavior under the applied voltage (Fig. S3 in the ESM). As can be seen, the change in ion conductance aligns with wettability, which is influenced by surface roughness and composition [33, 34]. We scanned the glass surface roughness using an atomic force microscope (AFM) and observed that the roughness changed only slightly with prolonged NaOH treatment durations, indicating that the glass surfaces are very flat (Fig. S4 in the ESM). Moreover, zeta potentials at solid–liquid interface show that longer soaking durations results in a gradual increase in negative potential, stabilizing at around –50 mV after 60 min (Fig. S5 in the ESM). It is well known that the negative potential arises from dissociation of silanol groups [35]. Therefore, the increase in glass hydrophilicity results from the increased density of –OH groups.

Furthermore, the height of liquid film nanochannels was estimated according to Eqs. (1)–(3) [12, 22]

$$G_{\mathrm{DLFN}} = \frac{2\pi r h}{L}\kappa \tag{1}$$

where r, h, L are the radius of the capillary, the height of the DLFN, and the length of the oil droplet, respectively. Conductivity κ is comprised of bulk solution conductivity κ_b and surface conductivity κ_s, the latter arising from two different interfaces—oil/water and water/solid. The surface conductivity can be expressed in the following form [36, 37]

$$\kappa_s = \frac{\mu(\sigma_1+\sigma_2)}{h}\left(1+\frac{e}{2\pi l_B \mu\eta}\right) \tag{2}$$

where μ, l_B, η, σ_1, and σ_2 are the ionic mobility, Bjerrum length, liquid viscosity, and charge density of oil/water and water/solid interfaces respectively.

Substituting Eq. (2) in Eq. (1), we obtain

$$h = \frac{\left[\frac{G^*_{\mathrm{DLFN}}}{2\pi r} - \mu(\sigma_1+\sigma_2)\left(1+\frac{e}{2\pi l_B \mu\eta}\right)\right]}{\kappa_b} \tag{3}$$

To eliminate the influence of variations in oil droplet length, we normalize the conductance of the film nanochannel per unit length, as $G^*_{\mathrm{DLFN}} = G_{\mathrm{DLFN}} \times L$. The formulas for the mobility (μ) and

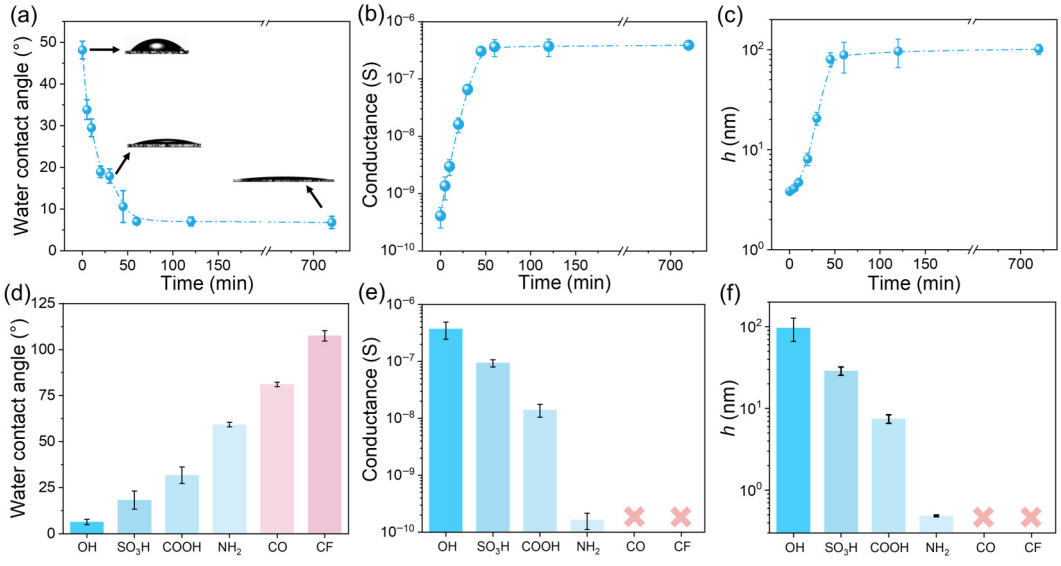

Figure 2 The effect of wettability on the height and ionic conductance of liquid film nanochannels. (a) Water contact angles on the flat glass treated with NaOH solution for varying durations. (b) Ion conductance and (c) estimated height of liquid film nanochannels constructed in capillaries treated with NaOH solution for various durations. (d) Water contact angles on flat glass modified with different functional groups. (e) Ion conductance and (f) estimated height of liquid film nanochannels constructed in capillaries modified with different functional groups. All the ion solution is 0.1 M KCl.

conductivity (σ) are provided in Note S1 in the ESM, where the physical constants can also be found. The zeta potential at the oil–water interface is approximately –17.8 mV, with hexadecane as the oil and a 0.1 M KCl solution.

As shown in Fig. 2(c), the estimated height of the liquid film nanochannels increases with longer NaOH treatment durations, stabilizing at around 100 nm after 60 min. In addition, snapshots of oil droplets in capillary show that the angles between the oil and the capillary decrease with extended NaOH treatment durations, which also indicate an increase in film thickness (Fig. S6 in the ESM) [12, 22]. In summary, it can be inferred that longer NaOH treatment durations lead to a higher density of –OH groups on the glass surface, which enhances hydrophilicity and consequently results in thicker liquid film and improved ion conductance.

In the above, wettability is regulated by adjusting the –OH density on the glass surface. However, the wettability range achieved by this method is limited, with water contact angles ranging from ~ 6° to ~ 50°. To investigate a wider wettability range, we modified different functional groups on the glass surface, achieving water contact angles from ~ 6° to ~ 110° (Fig. 2(d)). The modification process is shown in Fig. S7 in the ESM. Similarly, we characterized the ion conductance of liquid film nanochannels formed in capillaries modified with various functional groups (Fig. 2(e) and Fig. S8 in the ESM). The results show that as the hydrophobicity of capillary wall increases, the conductance of liquid film nanochannel decreases. Notably, no ion conductance was observed in capillaries modified with –CO and –CF. Furthermore, the height of the liquid film nanochannels was estimated using Eq. (3), and the zeta potentials at solid–liquid interface were characterized using SurPASS 3 (Fig. S9 in the ESM). The results indicate that as the hydrophobicity increases, the liquid film thickness decreases, and no liquid film nanochannels are present in capillaries modified with –CO and –CF (Fig. 2(f)). Additionally, snapshots of oil droplets in the capillaries show a transition in their appearance from convex to concave, which also indicates a decrease in film thickness (Fig. S10 in the ESM).

To explore the mechanism underlying the variation in liquid film thickness, we measured contact angles and adhesion force of underwater hexadecane on flat glass treated with NaOH solution for various durations. As shown in Fig. 3(a), the underwater contact angles of hexadecane increase with longer NaOH treatment durations, while its underwater adhesion force decreases from ~ 50 to ~ 0 μN (Fig. 3(b) and Fig. S11 in the ESM). These results indicate that the stability of the liquid film improves with extended NaOH treatment. However, on hydrophilic glass treated with NaOH solution for 30, 40 and 60 min, both the underwater adhesion force (~ 0 μN) and contact angles (~ 150°) of hexadecane remain similar. It is clear that macroscopic oil adhesion behaviors cannot reveal the variations in film thickness on hydrophilic surfaces. Therefore, we seek to reveal the underlying mechanism by analyzing the surface components of glass. According to the Owens–Wandt–Rabel–Kaelble (OWRK) method [38, 39], we measured the surface energy of flat glass treated with NaOH solution for various durations and categorized it into two components: dispersive (γ^d) and polar (γ^p) [27]. Furthermore, we define f as the ratio of the polar to dispersive components of surface energy, reflecting the proportion of surface polarity. Figure 3(c) shows that surface energy of glass surfaces increases with longer NaOH treatment durations, and the f value also trends upward. Combing surface energy and film thickness, it is apparent that the thickness of liquid film is regulated by the polar interaction between water and glass [40, 41]. Taking superhydrophilic glass surfaces (treated with NaOH solution for 60 min) and blank glass surfaces (treated with NaOH solution for 0 min) as examples: superhydrophilic glass surfaces are dominated by polar –OH components, exhibiting high affinity for water through hydrogen bonds, while the nonpolar hexadecane is repelled. Consequently, a thicker liquid film forms between hexadecane and superhydrophilic glass. However, blank glass surfaces contain fewer polar –OH groups, reducing its affinity for water and resulting in a thinner liquid film.

In fact, surface polarity affects the liquid film thickness by changing the structure of the interfacial water molecules. Studies have shown that the liquid film thickness is closely related to the

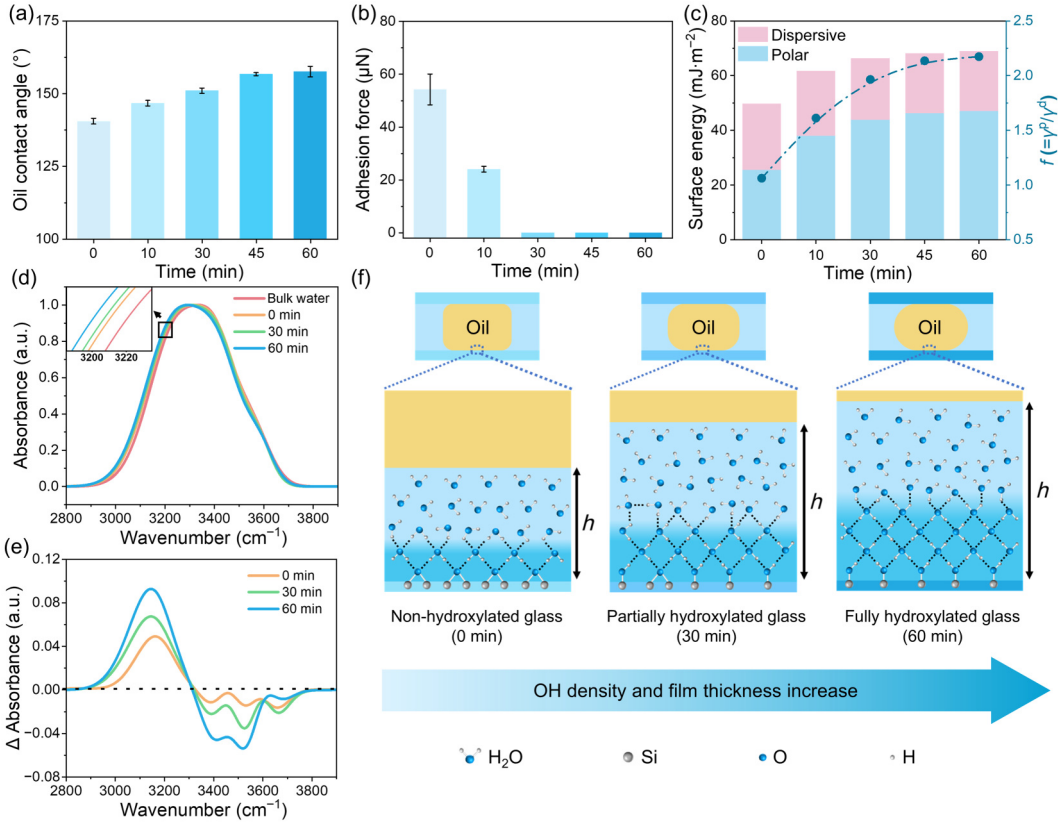

Figure 3 Mechanistic insights into the influence of wettability on liquid film thickness. (a) Underwater hexadecane contact angles and (b) adhesion force on the flat glass treated with NaOH solution for varying durations. (c) Surface energy of flat glass with polar and dispersive components. (d) ATR-IR spectra of bulk water and interfacial water at glass surface treated with NaOH solution for varying durations. (e) Difference spectra obtained by subtracting the spectrum of the bulk water. (f) Diagram illustrating the effect of interfacial water molecule arrangement at the surfaces of non-hydroxylated, partially hydroxylated and fully hydroxylated glass on the thickness of liquid film.

orientation and hydrogen bond structure of interfacial water molecules [42–44]. We select three glass surfaces treated with NaOH solution for 0, 30, 60 min to represent non-hydroxylated, partially hydroxylated and fully hydroxylated glass surfaces [45]. The –OH vibration frequency of interfacial water molecules at three glass surfaces were measured using ATR-IR spectroscopy [43]. Figure 3(d) and the insert diagram show that the proportion of tetrahedrally coordinated water increases with higher –OH density, indicating an enhanced hydrogen bonding network. To highlight the differences among the three systems and minimize the influence of bulk water, we propose the difference spectra by subtracting the spectrum of the bulk water [46, 47]. As shown in Fig. 3(e), the spectral changes in the O–H region around 3200 cm^{-1} significantly increase in intensity over time, accompanied by a decrease at around 3400 cm^{-1}. It has been reported that –OH vibration around 3200 cm^{-1} corresponds to tetrahedrally coordinated water that is involved in four hydrogen bonds, 3400 cm^{-1} represents water that is partially involved in hydrogen bonds but not fully coordinated, and 3600 cm^{-1} indicates free water that does not participate in hydrogen bonds [48, 49]. Therefore, it is clear that a higher density of polar –OH groups enhance the hydrogen bonding network of water molecules, resulting in a more stabilized liquid film. Three simplified models are proposed to explain the difference in liquid film thickness. As shown in Fig. 3(f), non-hydroxylated glass surfaces are predominantly composed by Si–O–Si components, exhibiting the lowest amount of strongly bound water and thin liquid film. In contrast, partially hydroxylated glass surfaces contain more –OH groups, leading to increased strongly bound water and a thicker liquid film. Fully hydroxylated glass surfaces, composed primarily of polar –OH groups, facilitate the retention of strongly bound water on the surface, resulting in thicker liquid film. Therefore, surface polarity and interfacial water conformation effectively explain the differences in liquid film thickness among various glass surfaces treated with NaOH solution for various durations.

Moreover, glass surfaces modified by different functional groups also exhibit a similar trend. As the glass surface transitions from superhydrophilic to hydrophobic, the underwater hexadecane contact angles decrease (Fig. S12 in the ESM), and the underwater adhesion force of hexadecane increases (Fig. S13 in the ESM). The surface energy and polarity component were tested using the OWRK method [38, 39] and the results indicate that the surface energy decreases as the glass surface changes from superhydrophilic to hydrophobic (Fig. S14 in the ESM). Superhydrophilic surfaces, dominated by polar components, bind water through hydrogen bonds, leading to a thicker liquid film. Conversely, hydrophobic surfaces, dominated by dispersion components, preferentially attract oil via hydrophobic interactions and repel water, resulting in the absence of a liquid film. Additionally, considering the effect of oil polarity on ion conductance, the results for other oils (n-octanol, n-octanoic acid, and toluene) are also discussed. In the superhydrophilic capillary, ionic conductance increases slightly as oil polarity decreases, due to hydrogen bonding interactions between the polar groups of the oil and the Si–OH groups on the

glass surface (Fig. S15 in the ESM). In contrast, in the hydrophobic capillary (modified with –CF), ionic conductance decreases as oil polarity decreases (Fig. S16 in the ESM), attributed to hydrophobic interactions between the nonpolar oil groups and the hydrophobic surface [50].

Based on the results above, wettability can regulate the thickness of the liquid film, thereby affecting ion transport. Therefore, continuous regulation of film thickness and ion transport can be achieved by constructing capillaries with gradient wettability. As shown in Fig. 4(a), a capillary was positioned vertically in a 0.1 M NaOH solution. It was immersed in zone 4 for 30 min, then in zone 3 for 20 min, followed by zone 2 for 10 min, while zone 1 was left untreated. Then, four different wettability regions were established on a capillary. By positioning the oil droplet in each of the four zones, DLFNs were created (Fig. 4(b)). The ion current measurements demonstrate that the DLFNs can regulate ion transport across four orders of magnitude while exhibiting good cyclic stability (Fig. 4(c)). Similarly, we generated a gradient wettability along the glass surface. Due to the limited viewing angle of the contact angle measurement system, we combined four photographs to capture the contact angles along the substrate (Fig. S17(a) in the ESM). Water contact angle measurements across the four wettability regions showed reversible changes from ~ 50° to ~ 6°, demonstrating good cycling stability (Fig. S17(b) in the ESM). Finally, we measured the ion conductance of DLFNs at varying KCl concentrations and observed a consistent trend (Figs. S18 and S19 in the ESM).

The DLFNs can be used for on-demand molecule delivery. Fluorescein sodium molecule is used as the model molecule, and its structure is shown in Fig. 5(a). We plotted standard curves of fluorescein sodium fluorescence intensity versus its corresponding concentration to determine the molecular concentration on the transport side (Fig. S20 in the ESM). First, we tested the molecular transport ability of four liquid film nanochannels, respectively.

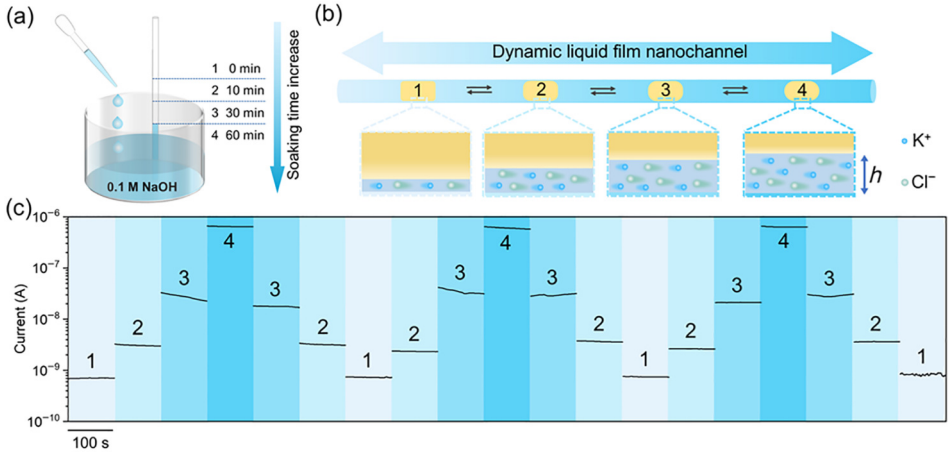

Figure 4 Construction of DLFNs. (a) Schematic diagram of the construction of capillary with gradient wettability. (b) Schematic diagram of DLFNs with multi-scale gating property. (c) Ion current cycling measurements of the DLFNs.

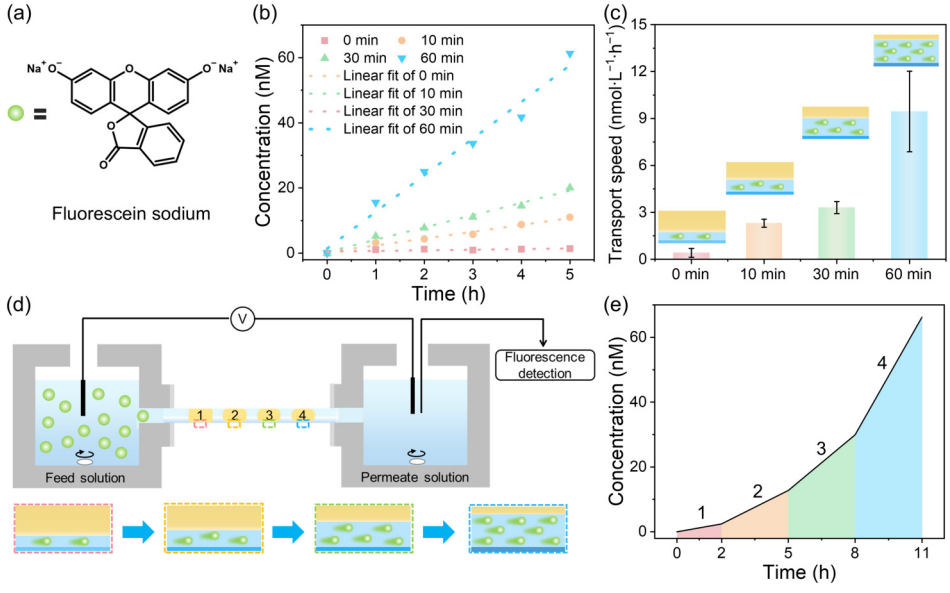

Figure 5 Application of the DLFNs for controlled molecule transport. (a) The structure of the fluorescein sodium molecule. (b) Fitting curves of concentration change over durations of fluorescein sodium passing through four kinds of liquid film nanochannels, which are constructed in capillaries treated with NaOH solution for 0, 10, 30 and 60 min, respectively. (c) Column graph of transport speed of fluorescein sodium passing through four kinds of liquid film nanochannels. (d) Schematic diagram of fluorescein sodium molecule transport through DLFNs with a driving voltage of +1 V (anode in the permeate side). (e) The four kinds of liquid film nanochannels are combined to obtain an on-demand molecule delivery curve over durations.

Figure 5(b) shows the concentration change of fluorescein sodium over time, with transport speeds calculated from the slope of the fitting curves (Fig. 5(c)). The results indicate that transport speed increases with longer NaOH treatment durations. Specifically, without NaOH treatment, the capillary exhibits low hydrophilicity, resulting in a thin liquid film and a low molecular transport rate. As the NaOH treatment duration increases, the capillary's hydrophilicity improves, leading to a thicker liquid film and a higher molecular transport rate. Finally, we combined the four liquid film nanochannels on a capillary for on-demand molecule deliver. As shown in Fig. 5(d), the capillary with gradient wettability was mounted between two PTFE reservoirs. In the left reservoir, 5 mL of 1 mM aqueous fluorescein sodium solution served as the feed solution, while the right reservoir contained 5 mL of deionized water as the permeate solution. Ag/AgCl electrodes were placed in both reservoirs (anode in the permeate side), and a constant potential of +1 V via a Keithley 6487 picoammeter was applied across the liquid film nanochannel to facilitate the transfer of fluorescein sodium molecules. Furthermore, both reservoirs were gently stirred with magnetic agitation to eliminate concentration gradients. Figure 5(e) shows the concentration curve of molecules over time, obtained from the DLFNs formed by placing the oil droplet in four distinct zones. The results indicate that molecular transport can be dynamically regulated at different transport rates.

4 Conclusion

In summary, we propose a simple and economic method for constructing DLFNs that enable the controlled transport of ions and molecules within an oil–water–solid three-phase system. The liquid film thickness can be dynamically regulated over 2–3 orders of magnitude by positioning the oil droplet within the varying wettability regions of the capillary. Experimental results indicate that the liquid film thickness is influenced by the interfacial water structure, which is mediated through hydrogen bonding interactions. Specifically, increased surface hydrophilicity enhances hydrogen bonding interactions between the glass surface and water, leading to a higher proportion of tetracoordinated water and thicker liquid film. Unlike solid-state nanochannels, which typically have two gate states: "open" and "closed", the DLFNs exhibit multiscale gating. Ionic conductance can be extensively tuned over four orders of magnitude, and molecular transport can be dynamically regulated at varying transport speeds. Our study introduces a convenient and cost-effective approach for constructing multiscale gating nanofluids, which hold potential applications in drug delivery, microreactors, sensing, and beyond.

Electronic Supplementary Material: Supplementary material (supporting Figs. S1–S20: including experimental setup, *I*–*V* curves, AFM images, microscope images, zeta potentials, chemical modification process, adhesion measurements, surface energy, ion conductance, bulk conductivity, and calibration curve of fluorescence intensity; supporting Notes: calculation of film thickness) is available in the online version of this article at https://doi.org/10.26599/NR.2025.94907256.

Data availability

All data needed to support the conclusions in the paper are presented in the manuscript and the Electronic Supplementary Material.

Acknowledgements

This research is supported by the National Natural Science Foundation of China (No. 22090052), Frontier Science Key Projects of CAS (No. ZDBS-LY-SLH022), Key R&D Project of Shandong Province (No. 2022CXGC010302), and Xiaomi Young Talents Program.

Declaration of competing interest

All the contributing authors report no conflict of interests in this work.

Author contribution statement

Y. T. conceived the project. Y. T., C. X. L., and D. Y. W. designed the experiments, and C. X. L. performed the experiments. C. X. L., D. Y. W., Z. X., H. T. D., and F. X. discussed and analyzed the data. C. X. L. drafted the manuscript and Y. T. revised the manuscript. All authors contributed to the general discussion.

Use of AI statement

None.

References

[1] Sheng, Z. Z.; Zhang, M. C.; Liu, J.; Malgaretti, P.; Li, J. Y.; Wang, S. L.; Lv, W.; Zhang, R. R.; Fan, Y.; Zhang, Y. M. et al. Reconfiguring confined magnetic colloids with tunable fluid transport behavior. *Natl. Sci. Rev.* **2021**, *8*, nwaa301.

[2] Wang, C.; Wang, D. Y.; Miao, W. N.; Shi, L. X.; Wang, S. T.; Tian, Y.; Jiang, L. Bioinspired ultrafast-responsive nanofluidic system for ion and molecule transport with speed control. *ACS Nano* **2020**, *14*, 12614–12620.

[3] Wang, C.; Wang, D. Y.; Miao, W. N.; Tian, Y. Intelligent controllable microreactor based on superhydrophilic nanochannel. *Chem. J. Chin. Univ.* **2021**, *42*, 1276–1283.

[4] Qiu, M.; Zhu, Z. P.; Wang, D. Y.; Xu, Z.; Xia, F.; Jiang, L.; Tian, Y. Superspreading-confined assembly of oriented 2D MOF membranes for biomimetic cation-regulated ion transport. *Adv. Funct. Mater.* **2024**, *34*, 2316040.

[5] Liu, Y. L.; Yu, S. Y.; An, R. B.; Miao, Y. X.; Jiang, D. C.; Ye, D. J.; Xu, J. J.; Zhao, W. W. A fast and reversible responsive bionic transmembrane nanochannel for dynamic single-cell quantification of glutathione. *ACS Nano* **2023**, *17*, 17468–17475.

[6] Fan, Y.; Sheng, Z. Z.; Chen, J.; Pan, H.; Chen, B. Y.; Wu, F.; Wang, S. L.; Chen, X. Y.; Hou, X. Visual chemical detection mechanism by a liquid gating system with dipole-induced interfacial molecular reconfiguration. *Angew. Chem., Int. Ed.* **2019**, *58*, 3967–3971.

[7] Wang, H. M.; Fan, Y.; Hou, Y. Q.; Chen, B. Y.; Lei, J. M.; Yu, S. J.; Chen, X. Y.; Hou, X. Host–guest liquid gating mechanism with specific recognition interface behavior for universal quantitative chemical detection. *Nat. Commun.* **2022**, *13*, 1906.

[8] Zhang, Y. M.; Han, Y. H.; Ji, X. L.; Zang, D. Y.; Qiao, L.; Sheng, Z. Z.; Wang, C. Y.; Wang, S. L.; Wang, M.; Hou, Y. Q. et al. Continuous air purification by aqueous interface filtration and absorption. *Nature* **2022**, *610*, 74–80.

[9] Li, J.; Shi, Y. Y.; Qi, C. Y.; Zhang, B. W.; Xing, X. W.; Li, Y. L.; Chen, T. D.; Mao, X. N.; Zuo, Z. J.; Zhao, X. L. et al. Charging metal-organic framework membranes by incorporating crown ethers to capture cations for ion sieving. *Angew. Chem., Int. Ed.* **2023**, *62*, e202309918.

[10] Wang, Y.; Yang, T.; Bao, C. Y.; Xu, X. L.; Zhang, J. Y.; Peng, B.; Luo, X. Z.; Wang, B. Y.; Luo, C.; Wang, Y. J. et al. Charged cyclodextrin membranes for precise molecular sieving. *J. Mater.*

Chem. A **2022**, *10*, 22301–22310.
[11] Hou, X.; Hu, Y. H.; Grinthal, A.; Khan, M.; Aizenberg, J. Liquid-based gating mechanism with tunable multiphase selectivity and antifouling behaviour. *Nature* **2015**, *519*, 70–73.
[12] Liang, C. X.; Wang, D. Y.; He, S. F.; Zhang, L.; Xia, F.; Tian, Y. Bioinspired cation-gated dynamic liquid film nanochannel for controlled transport of ions and molecules. *Sci. China Mater.* **2024**, *67*, 2523–2531.
[13] Zhang, M. C.; Xing, C.; Huang, J. N.; Li, P. S.; Jiang, L.; Liu, L. F.; Jia, J. B.; Zhang, X. W.; Zhang, S. Q.; Liu, C. Y. Adaptive gating enhances intelligent membranes for cellular functions and precise separations. *Adv. Funct. Mater.* **2024**, *34*, 2310647.
[14] Lin, K. B.; Lin, C. Y.; Polster, J. W.; Chen, Y. F.; Siwy, Z. S. Charge inversion and calcium gating in mixtures of ions in nanopores. *J. Am. Chem. Soc.* **2020**, *142*, 2925–2934.
[15] Hou, X.; Yang, F.; Li, L.; Song, Y. L.; Jiang, L.; Zhu, D. B. A biomimetic asymmetric responsive single nanochannel. *J. Am. Chem. Soc.* **2010**, *132*, 11736–11742.
[16] Gu, R. X.; de Groot, B. L. Central cavity dehydration as a gating mechanism of potassium channels. *Nat. Commun.* **2023**, *14*, 2178.
[17] Powell, M. R.; Cleary, L.; Davenport, M.; Shea, K. J.; Siwy, Z. S. Electric-field-induced wetting and dewetting in single hydrophobic nanopores. *Nat. Nanotechnol.* **2011**, *6*, 798–802.
[18] Polster, J. W.; Aydin, F.; de Souza, J. P.; Bazant, M. Z.; Pham, T. A.; Siwy, Z. S. Rectified and salt concentration dependent wetting of hydrophobic nanopores. *J. Am. Chem. Soc.* **2022**, *144*, 11693–11705.
[19] Zhou, Y. H.; Hao, J. R.; Zhou, J. J.; Liao, J. W.; Wei, Y.; Chen, X. C.; Ning, C. Y.; Deng, X. L.; Jiang, L. Dynamically modulated gating process of nanoporous membrane at sub-2-nm speed. *Matter* **2022**, *5*, 281–290.
[20] Wu, Y. F.; Yang, G.; Lin, M. C.; Kong, X. Y.; Mi, L.; Liu, S. Q.; Chen, G. S.; Tian, Y.; Jiang, L. Continuously tunable ion rectification and conductance in submicrochannels stemming from thermoresponsive polymer self-assembly. *Angew. Chem., Int. Ed.* **2019**, *58*, 12481–12485.
[21] Miao, W. N.; Tian, S. H.; Yuan, Q. Z.; Tian, Y.; Jiang, L. Direct observation of spreading precursor liquids in a corner. *Natl. Sci. Rev.* **2023**, *10*, nwad119.
[22] Ma, Y.; Sun, M.; Duan, X. X.; van den Berg, A.; Eijkel, J. C. T.; Xie, Y. B. Dimension-reconfigurable bubble film nanochannel for wetting based sensing. *Nat. Commun.* **2020**, *11*, 814.
[23] Rabinowitz, J.; Whittier, E.; Liu, Z.; Jayant, K.; Frank, J.; Shepard, K. Nanobubble-controlled nanofluidic transport. *Sci. Adv.* **2020**, *6*, eabd0126.
[24] Zhang, S. P.; Song, R. Y.; Zeng, H. O.; Wu, N. R.; Duan, H. W.; Wang, L. D. Exploring anomalous nanofluidic transport at the interfaces. *Droplet* **2024**, *3*, e110.
[25] Wang, Z.; Guo, L. F.; Xiao, H. Y.; Cong, H.; Wang, S. T. A reversible underwater glue based on photo- and thermo-responsive dynamic covalent bonds. *Mater. Horiz.* **2020**, *7*, 282–288.
[26] Liu, G. C.; Gao, M. J.; Chen, W.; Hu, X. Y.; Song, L. B.; Liu, B.; Zhao, Y. D. Ph-modulated ion-current rectification in a cysteine-functionalized glass nanopipette. *Electrochem. Commun.* **2018**, *97*, 6–10.
[27] He, S. F.; Zhu, Z. P.; Zhang, B.; Tian, Y. Wetting thresholds for long-lasting superwettability: From intrinsic wetting boundary to critical roughness value. *Chem. Eng. J.* **2023**, *454*, 140058.
[28] Hao, D. Z.; Wang, Z.; Liu, M. J.; Guo, X. L.; Wang, S. T.; Jiang, L. Strong anchoring of hydrogels through superwetting-assisted high-density interfacial grafting. *Angew. Chem., Int. Ed.* **2023**, *62*, e202215034.
[29] Zhu, Z. P.; Tian, Y.; Chen, Y. P.; Gu, Z.; Wang, S. T.; Jiang, L. Superamphiphilic silicon wafer surfaces and applications for uniform polymer film fabrication. *Angew. Chem., Int. Ed.* **2017**, *56*, 5720–5724.
[30] Parida, S. K.; Dash, S.; Patel, S.; Mishra, B. K. Adsorption of organic molecules on silica surface. *Adv. Colloid Interface Sci.* **2006**, *121*, 77–110.
[31] Michalske, T. A.; Freiman, S. W. A molecular mechanism for stress-corrosion in vitreous silica. *J. Am. Ceram. Soc.* **1983**, *66*, 284–288.
[32] Bunker, B. C. Molecular mechanisms for corrosion of silica and silicate glasses. *J. Non-Cryst. Solids* **1994**, *179*, 300–308.
[33] Tian, Y.; Jiang, L. Intrinsically robust hydrophobicity. *Nat. Mater.* **2013**, *12*, 291–292.
[34] Liu, M. J.; Wang, S. T.; Jiang, L. Nature-inspired superwettability systems. *Nat. Rev. Mater.* **2017**, *2*, 17036.
[35] Behrens, S. H.; Grier, D. G. The charge of glass and silica surfaces. *J. Chem. Phys.* **2001**, *115*, 6716–6721.
[36] Levine, S.; Marriott, J. R.; Robinson, K. Theory of electrokinetic flow in a narrow parallel-plate channel. *J. Chem. Soc., Faraday Trans. 2* **1975**, *71*, 1–11.
[37] Bocquet, L.; Charlaix, E. Nanofluidics, from bulk to interfaces. *Chem. Soc. Rev.* **2010**, *39*, 1073–1095.
[38] Owens, D. K.; Wendt, R. C. Estimation of the surface free energy of polymers. *J. Appl. Polym. Sci.* **1969**, *13*, 1741–1747.
[39] Schlisske, S.; Held, M.; Rödlmeier, T.; Menghi, S.; Fuchs, K.; Ruscello, M.; Morfa, A. J.; Lemmer, U.; Hernandez-Sosa, G. Substrate-independent surface energy tuning via siloxane treatment for printed electronics. *Langmuir* **2018**, *34*, 5964–5970.
[40] Shi, C.; Yan, B.; Xie, L.; Zhang, L.; Wang, J. Y.; Takahara, A.; Zeng, H. B. Long-range hydrophilic attraction between water and polyelectrolyte surfaces in oil. *Angew. Chem., Int. Ed.* **2016**, *55*, 15017–15021.
[41] Wang, Y.; Di, J. C.; Wang, L.; Li, X.; Wang, N.; Wang, B. X.; Tian, Y.; Jiang, L.; Yu, J. H. Infused-liquid-switchable porous nanofibrous membranes for multiphase liquid separation. *Nat. Commun.* **2017**, *8*, 575.
[42] Asay, D. B.; Kim, S. H. Evolution of the adsorbed water layer structure on silicon oxide at room temperature. *J. Phys. Chem. B* **2005**, *109*, 16760–16763.
[43] Chen, L.; He, X.; Liu, H. S.; Qian, L. M.; Kim, S. H. Water adsorption on hydrophilic and hydrophobic surfaces of silicon. *J. Phys. Chem. C* **2018**, *122*, 11385–11391.
[44] Chen, L.; Ngo, D.; Luo, J. W.; Gong, Y. F.; Xiao, C.; He, X.; Yu, B. J.; Qian, L. M.; Kim, S. H. Dependence of water adsorption on the surface structure of silicon wafers aged under different environmental conditions. *Phys. Chem. Chem. Phys.* **2019**, *21*, 26041–26048.
[45] Argyris, D.; Cole, D. R.; Striolo, A. Dynamic behavior of interfacial water at the silica surface. *J. Phys. Chem. C* **2009**, *113*, 19591–19600.
[46] Joutsuka, T.; Morita, A. Improved theory of difference vibrational spectroscopy and application to water. *J. Chem. Theory Comput.* **2016**, *12*, 5026–5036.
[47] Lin, Z. Q.; Saito, H.; Sato, H.; Sugimoto, T. Positive and negative impacts of interfacial hydrogen bonds on photocatalytic hydrogen evolution. *J. Am. Chem. Soc.* **2024**, *146*, 22276–22283.
[48] Shen, L. F.; Lu, B. A.; Li, Y. Y.; Liu, J.; Huang-Fu, Z. C.; Peng, H.; Ye, J. Y.; Qu, X. M.; Zhang, J. M.; Li, G. et al. Interfacial structure of water as a new descriptor of the hydrogen evolution reaction. *Angew. Chem., Int. Ed.* **2020**, *59*, 22397–22402.
[49] Li, C. Y.; Le, J. B.; Wang, Y. H.; Chen, S.; Yang, Z. L.; Li, J. F.; Cheng, J.; Tian, Z. Q. *In situ* probing electrified interfacial water structures at atomically flat surfaces. *Nat. Mater.* **2019**, *18*, 697–701.
[50] Liu, F. H.; Yang, H.; Wang, J. Y.; Zhang, M. H.; Chen, T.; Hu, G. X.; Zhang, W.; Wu, J. Z.; Xu, S. J.; Wu, X. et al. Salinity-dependent adhesion of model molecules of crude oil at quartz surface with different wettability. *Fuel* **2018**, *223*, 401–407.